Splenic T follicular helper cells compromise *Mycobacterium tuberculosis* clearance in aged C57BL/6 mice

Running Title: Immune response in aged host

Falak Pahwa[1], Shweta Chaudhary[1], Shivam Chaturvedi[2], Ranjan Kumar Nanda[1*]

[1]Translational Health Group, International Centre for Genetic Engineering and Biotechnology, New Delhi-110067, India

[2]Bio-experimentation Facility, International Centre for Genetic Engineering and Biotechnology, New Delhi-110067, India

*__Corresponding author:__

Ranjan Kumar Nanda (Ph.D.)

Translational Health Group, International Centre for Genetic Engineering and Technology, New Delhi-110067, India

Telephone: 91-11-26741358

Fax: 91-11-26742316

Email: ranjan@icgeb.res.in

Abstract

Ageing increases susceptibility to infectious diseases like tuberculosis (TB), however limited reports are available on the cellular and molecular details in aged (>60 years) patients. In this study, we asked how low aerosol dose of *Mycobacterium tuberculosis* H37Rv (Mtb) affects aged (17/19 months; M) C57BL/6 mice in their bacterial clearance, liver micronutrient levels, circulatory cytokines and T cell distribution compared to younger (2/4M) controls. Till 6 weeks post infection, aged mice showed similar tissue (lung, spleen, and liver) Mtb load as young mice. Interestingly, aged mice showed a delayed lung Mtb clearance at 2 weeks post rifampicin (RIF) - isoniazid (INH) treatment compared to younger mice. Aged mice showed unregulated liver Fe levels upon Mtb infection while young mice had lower Fe levels. Aged Mtb infected mice revealed a lower proportion of splenic T-follicular helper (T_{FH}) like $CD4^+$ T cells, which provides B cell help in generating high affinity antibodies and immune memory. Aged mice had higher basal circulatory IL-6 levels. Circulatory IFN-γ levels in aged (19M) C57BL/6 mice failed to resolve upon RIF-INH treatment. Splenic $CD4^+CD44^+$ T cells of aged mice showed deregulated levels of mitochondrial proteins (4-hydroxy-2-oxoglutarate aldolase and aspartate aminotransferase). Overall, while filling in knowledge gaps on the host age-related responses to Mtb infection and during treatment, this study provides new perspectives for T cell distribution and function, which opens avenue for adjunct therapeutic development for geriatric TB patients.

Keywords: Ageing, Immunosenescence, T cells, T_{FH} cells, Tuberculosis, Proteomics

Introduction

Age-related immunosenescence causes loss of immune competence leading to a reduced vaccine efficacy and increased susceptibility to various infectious diseases like influenza, pneumonia, bronchitis, and tuberculosis (TB)[1,2]. TB is caused by *Mycobacterium tuberculosis* (Mtb) infection and geriatric population (>65 years) accounted for the highest TB incidence rate (4 per 100,000 persons) in the United States[3]. Other than being a large reservoir of TB, aged patients also report with atypical presentation (including sputum smear-negative pulmonary involvement) and high mortality rate (14.94 per 100,000 infected people in 2017)[2,4,5,6]. Understanding immune responses of aged host is key to develop strategies that might improve the compromised immune system and will be useful for TB disease management.

Many mice strains like C57BL/6, BALB/c, C3HeB/FeJ of 6-8 weeks of age which is equivalent to human of 18-20 years, are commonly used by researchers to delineate TB pathophysiology[7]. Aged (24 months) AB6F1 and B6D2F1 mice control low dose of Mtb infection at early time point (upto 8 weeks) and succumb to the infection at later time points[8,9]. This is partly attributed to a higher $CD8^+$ T cell frequency and delayed antigen-specific $CD4^+$ T cell responses[10,11]. There still remains a knowledge gap in molecular mechanisms that explain a decline in immune responses to microbial i.e. bacterial and viral infections with age and their response to treatment. Characterizing altered immune cell subsets and their function in aged host might be useful to identify targets for adjunct therapeutics development.

In this study, we asked how differently aged (17/19 months; >60 years of human age) and young (2/4 months; 18-20 years in human) C57BL/6 mice respond in the initial time points of low aerosol dose Mtb infection and upon treatment. We monitored tissue Mtb burden, and aimed to correlate changes in immunological repertoire of young and aged C57BL/6 mice and deregulation at cellular and tissue level including circulation. A delayed lung Mtb clearance was observed in aged mice at 2 weeks post treatment compared to younger mice. Aged mice showed higher liver Cu/Zn and circulatory IL-6 levels, implying a higher inflammatory state. Aged Mtb infected mice demonstrated declined splenic T_{FH}-like ($CD4^+CD44^+CXCR5^+PD1^+$) cells at 6 weeks post infection. Functional characterization of splenic $CD4^+CD44^+$ T cells of aged mice at proteome level revealed deregulation in mitochondrial proteins 4-hydroxy-2-oxoglutarate aldolase and aspartate aminotransferase. Taken together, our data demonstrate higher inflammation, altered immune cell distribution and dysfunction leading to delayed Mtb clearance in aged C57BL/6 mice, which will be useful to develop interventions for geriatric TB patients.

Results

Aged (17M), male C57BL/6 mice showed compromised lung Mtb clearance at 2 weeks of treatment (RIF-INH): Prevalence of TB in males is four times higher than females[12]. Male C57BL/6 mice show higher susceptibility to Mtb infection with accelerated disease progression and premature death compared to females[13]. In this study, male C57BL/6 mice of 2M and 17M age groups were infected with low aerosol dose (100-120 cfu) of Mtb (Fig. 1A). Pre-infection, 17M C57BL/6 mice had higher (1.23×, $p<0.0001$) body weight than 2M mice (Fig. 1B). Healthy 2M mice showed ~8% increase within 6 weeks, as compared to 17M control mice that lost 3% body weight (Fig. 1C). Mtb infected 17M mice showed significant loss of body weight (~4%) by 2 w.p.i. while it was marginal in 2M mice (Fig. 1C). It seems that Mtb infected 2M mice showed marginal changes in their body weight and contained the infection efficiently by 2 w.p.i.. At 4 w.p.i., 2M mice showed ~6% ($p=0.02$) body weight loss while 17M mice lost ~3.5% weight ($p=0.08$) as compared to their healthy counterparts (Fig. 1C). By 6 w.p.i., 17M mice lost ~8% of their body weight which contributed to a worsened TB pathophysiology. Interestingly, by 2 w.p.t. with RIF-INH, Mtb infected 17M mice regained their lost body weight (Supplementary Fig. S1).

Tissue (lung, spleen, and liver) gross pathology was equally affected in Mtb infected 2M and 17M mice (Fig. 1D and Supplementary Fig. S2). Mice of both age groups receiving RIF-INH, showed clear lungs, similar spleen and liver size (Fig 1D, Supplementary Figs. S3 and S4). Lung histopathology of Mtb infected mice of both age groups revealed multiple foci of inflammatory cells and granulomatous lesions, without necrosis (Fig. 1E and Supplementary Fig. S5). However, prominent foamy cells in the lungs of 2M mice were observed by 4 w.p.i., while in 17M mice was observed at 6 w.p.i.. As expected, at 6 w.p.i. the lung histopathological score was maximum in both the age groups, which were resolved by 4 w.p.t. (Fig. 1E). Spatio temporal adaptation of Mtb in the liver of 2M and 17M mice resulted in mild hydropic degenerative changes with higher number of inflammatory cells, which were resolved by 2 w.p.t. (Fig. 1F and Supplementary Fig. S5).

Aged immune system of 17M mice might show a higher mycobacterial load in the affected pulmonary and extra-pulmonary sites. However, the tissue (lung, spleen and liver) Mtb burden remained similar till 6 w.p.i. in both the age groups (Figs. 1G, H and I). A time dependent increase in lung Mtb load was observed, which peaked at 4 w.p.i. and plateaued by 6 w.p.i. in both the age groups, corroborating earlier reports[8,9]. Interestingly, 17M mice receiving RIF-INH treatment showed a delayed lung mycobacterial clearance (two out of five mice showed ~3 $\log_{10}$ cfu) at the early time point (2 w.p.t.) as compared to 2M group (~1.2 $\log_{10}$ cfu, Fig.

1G). By 4 w.p.t., lung Mtb load in 2M and 17M mice were below the limit of detection (LOD) and by 2 w.p.t., it was below LOD in the spleen and liver (Figs. 1G, H, I). Upon Mtb infection, aged mice lost higher body weight presenting with worsened pathophysiology, along with a compromised lung mycobacterial clearance at early treatment phase compared to younger mice.

Deregulated micronutrient balancing observed in Mtb infected 17M C57BL/6 mice: Trace metals act as cofactors for various enzymatic functions and are essential for systemic, cellular and tissue immune responses in aged mice[14]. Liver enzymes are responsible for metabolising xenobiotic compounds including TB drugs and older TB patients are more prone to drug induced liver injury (DILI)[15,16]. Therefore, we hypothesized that the initial delay in lung mycobacterial clearance observed in aged mice might be partially attributed to the liver micronutrient imbalance. Thus, we estimated liver micronutrient levels of Mtb infected and control mice of both the age groups at 4 w.p.i. or 2 w.p.t. (Figs. 2A and B). Higher hepatic Cu (17M/2M=4.28×, $p<0.0001$) and low Zn (17M/2M=0.14×, $p<0.0001$), thus a high Cu/Zn with similar Fe (0.99×, $p=0.98$) and Se (0.77×, $p=0.08$) levels were observed in aged mice (Figs. 2C, D, E, F and G). At 4 w.p.i., hepatic Zn ($p=0.04$), Fe ($p=0.05$), and Se ($p=0.05$) levels were lower in 2M mice but remained similar in 17M mice compared to healthy controls (Figs. 2D, F and G). Infected host lowers available iron pool to limit Mtb growth and multiplication in young mice and reflected by the declined hepatic Fe levels[17,18]. Upon RIF-INH treatment, i.e. at 2 w.p.t. only 17M mice showed higher hepatic Cu ($p=0.02$), Zn ($p=0.02$) and Se ($p=0.03$) (Figs. 2C, D and G). Our findings, indicate that the observed imbalance in liver micronutrient profile in aged mice might be contributing to the compromised lung Mtb clearance at 2 w.p.t..

Splenic T_{FH} cell frequency decreased in Mtb infected 17M C57BL/6 mice: $CD4^+$ T cells controls bacterial infection like of Mtb[19]. While Th1 cells have been well studied, our understanding of T_{FH} cells, which link humoral and adaptive immunity, is still in its infancy. Aged mice upon Mtb infection are known to alter T cell repertoire, however limited reports explained anti-TB treatment-induced variations. Thus, we monitored immune cell frequency with markers for T cell activation (CD44), senescence (KLRG1, PD1) and homing receptor (CXCR5, typically expressed on T_{FH}) in the spleen and lungs. Splenocytes harvested from Mtb infected and control mice groups were processed and profiled using flow cytometry (Figs. 3A, B and C). 17M control mice had lower splenic $CD4^+$ T cells with higher CXCR5 and PD1 expression in both total and activated T cells compared to younger controls (Supplementary Figs. S6, A-K). $CD4^+KLRG1^+$, $CD4^+CD44^+KLRG1^+$ and $CD4^+CD44^+KLRG1^+PD1^+$ splenic cell frequencies were similar in both the age groups (Supplementary Figs. S6, J-L). We asked

whether the expression of these surface markers altered upon Mtb infection and during RIF-INH treatment. Mtb infected 2M and 17M mice showed similar total splenic $CD4^+$ T cell population (Fig. 3D), which corroborates earlier report on Mtb Erdman strain infected C57BL/10 mice of multiple age groups (3, 6, 12, 24M)[20]. A decline in splenic $CD4^+CD44^+$ cells was observed with infection progression in 17M mice while splenic $CD4^+CXCR5^+$ T cells increased in both the age groups (Fig. 3E and Supplementary Fig. S7B). Interestingly, $CD4^+CD44^+CXCR5^+$ T cells showed a time dependent increase in Mtb infected 2M mice but an inverse pattern was observed in 17M mice (Fig. 3F). $CD4^+PD1^+$, $CD4^+KLRG1^+$, $CD4^+CD44^+PD1^+$ and $CD4^+CD44^+KLRG1^+$ cells remained similar at both time points in Mtb infected 2M and 17M mice (Fig. 3G and Supplementary Figs. S7, C-E). However, overall higher $CD4^+PD1^+$ T cells were observed in 17M mice at 4 and 6 w.p.i. compared to 2M mice (Supplementary Fig. S7C). With infection progression, $CD4^+CXCR5^+PD1^+$ cell frequency increased in Mtb infected mice groups but was overall higher in 17M mice than 2M mice (Fig. 3H). In Mtb infected 17M mice, $CD4^+CD44^+CXCR5^+PD1^+$ (T_{FH}) cells decreased from 4 to 6 w.p.i. but remained similar at both the time points in 2M mice (Fig. 3I). Also, $CD4^+CD44^+CXCR5^+$ subset of Mtb infected 17M mice showed higher proportion of $PD1^+$ cells compared to $CD4^+CD44^+CXCR5^-$ subset (Fig. 3C). At 4 w.p.i., 2M mice had significantly low $CD4^+CD44^+KLRG1^+PD1^+$ cells compared to 17M group but decreased with time in 17M mice (Supplementary Fig. S7F). Post 4 weeks of post RIF-INH treatment, 17M mice had higher splenic $CD4^+CD44^+$, $CD4^+CXCR5^+$, $CD4^+CD44^+CXCR5^+$, $CD4^+PD1^+$, $CD4^+CD44^+PD1^+$ cell frequencies with low $CD4^+CXCR5^+PD1^+$ cells than 2M mice (Supplementary Figs. S8, A-H). However, $CD4^+CD44^+CXCR5^+PD1^+$ cells remain similar in both the age groups of mice receiving treatment (Supplementary Fig. S8I). $CD4^+KLRG1^+$ and $CD4^+CD44^+KLRG1^+PD1^+$ cells were higher in 17M treated mice compared to young mice, however $CD4^+CD44^+KLRG1^+$ cells were similar between the treated mice groups (Supplementary Figs. S8, J-L). Earlier report demonstrated reduced KLRG1 expression on $CD4^+$ and $CD8^+$ T cells in mice receiving RIF and INH treatment[21]. KLRG1 is a T cell differentiation indicator in murine TB, and higher KLRG1 expression observed in aged RIF and INH treated mice indicates that Mtb is priming terminal differentiation of the effector memory cells, which restricts their migration to the lungs[22]. As a result of low splenic T_{FH} and high $CD4^+CD44^+KLRG1^+PD1^+$ cells, aged mice showed a compromised Mtb clearance upon treatment as compared to younger counterpart.

Mtb infected lungs of both age groups have similar abundance of $CD4^+CXCR5^+PD1^+$ cells: T_{FH}-like cells are reported in mouse model of lung inflammation, which drives the local generation of germinal centre (GC)-like B cells and plasmablasts thus, producing antibodies in

the inflamed lungs[23]. Due to the observed low splenic $CD4^+CD44^+CXCR5^+PD1^+$ cell frequency in aged mice, we monitored these cells in the lungs to understand how the two mice age groups respond to the same dose of Mtb infection. The experimental strategy adopted for infection, lung immune cell isolation and gating strategies to profile the immune cells using flow cytometry from different mice groups are presented (Figs. 4A, B and C). The total lung $CD4^+$ T cells of Mtb infected mice of both the age groups significantly increased with time but 17M mice had overall lower frequency (17M/2M=0.74×, p=0.02) at 6 w.p.i. (Fig. 4D). $CD4^+CD44^+$ T cells were significantly higher (17M/2M=1.64×, p=0.03) in 17M mice at 4 w.p.i. while increased frequency of $CD4^+CD44^+$ T cells was observed in 2M group with infection progression (Fig. 4E). Lung $CD4^+CXCR5^+$ T cell frequency increased with infection progression from 4 to 6 w.p.i. in both the age groups (Supplementary Fig. S9B). Higher (1.93×, p=0.05) $CD4^+CD44^+CXCR5^+$ T cells were observed in 17M mice at 6 w.p.i. compared to 2M group (Fig. 4F). These $CD4^+CD44^+CXCR5^+$ T cells are reported to be accumulated in the lungs of Mtb infected 2M C57BL/6 mice and non-human primates[24]. Frequencies of $PD1^+$ and $KLRG1^+$ on total and activated $CD4^+$ T cells were found to be similar at 4 and 6 w.p.i. in both 2M and 17M mice groups (Fig. 4G and Supplementary Figs. S9, C-E). T_{FH}-like $CD4^+CXCR5^+PD1^+$ cell frequency increased with infection progression in both mice age groups (Fig. 4H). $CD4^+CD44^+KLRG1^+PD1^+$ cells declined significantly (p<0.0001) in 17M mice by 6 w.p.i., but remain unchanged in 2M group (Supplementary Fig. S9F). Thus, irrespective of the mice age, we observed that the Mtb load as well as T_{FH}-like cells in the lungs of the infected groups were similar.

Higher circulatory IL-6 and IFN-γ levels observed in 19M C57BL/6 mice: In another set of experiment, we used age groups (4M and 19M) of male C57BL/6 mice and monitored cfu and immune cell distribution at early time point i.e. 4 w.p.i. and 2 w.p.t. (Fig. 5A). The lung mycobacterial load at 4 w.p.i. in C57BL/6 mice was found to be similar for both 4M and 19M groups (Fig. 5B). Overall higher splenic Mtb load was observed in 4M C57BL/6 mice than 19M group which had cfu lower than LOD in two out of four mice (Fig. 5C). C57BL/6 mice of both age groups receiving RIF-INH treatment showed comparable splenic Mtb load at 2 w.p.t. (Fig. 5C). Pre-infection, 19M C57BL/6 mice had significantly higher body weight (1.23x, p<0.0001) than 4M group (Supplementary Fig. S10A). There were no significant changes in body weight in the two age groups of C57BL/6 mice upon Mtb infection at 4 w.p.i. and RIF- INH treatment at 2 w.p.t. (Supplementary Figs. S10, B-D). Tissue (lung, spleen, and liver) gross pathology and histopathology of lung and liver of Mtb infected 4M and 19M mice showed similar observations as in 2M and 17M C57BL/6 mice (Supplementary Figs. S11 and

S12). Mtb infected 19M C57BL/6 mice receiving RIF-INH treatment showed a marginal delay in bacterial clearance (~2 $\log_{10}$ cfu) at 2 w.p.t. as compared to 2M (~1 $\log_{10}$cfu) group (Fig. 5B).

The circulatory cytokines of both the mice age groups and different conditions were further monitored using LEGENDplex (Supplementary Fig. S13). Circulatory IL-6 levels were higher in healthy, Mtb infected and RIF-INH treated 19M C57BL/6 mice than 4M mice group (Fig. 5D). Circulatory IFN-γ levels were similar between 19M and 4M mice but it significantly increased upon Mtb infection in both the age groups (Fig. 5E). Post RIF-INH treatment, IFN-γ levels showed decreasing trends, however 19M C57BL/6 mice had higher levels at 2 w.p.t. (Fig. 5E). Circulatory TNF-α and IL-1β levels were higher in Mtb infected 4M and 19M C57BL/6 mice compared to their healthy counterparts (Figs. 5F and G). 4M C57BL/6 mice receiving RIF-INH treatment showed declined TNF-α and IL-1β levels while 17M mice showed similar TNF-α and even higher IL-1β levels compared to Mtb infected C57BL/6 mice (Figs. 5F and G). Circulatory IL-17A and IL-23 levels did not show any study group specific differences (Figs. 5H and I).

Higher splenic $CD4^+CD44^+CXCR5^+PD1^+ICOS^+$ cells observed in 19M C57BL/6 mice irrespective of their Mtb infection status: In 19M C57BL/6 mice, total splenic $CD4^+$ T cells remained similar after Mtb infection and post RIF-INH treatment (Supplementary Fig. S14A). Whereas, 4M C57BL/6 mice receving RIF-INH treament showed higher splenic $CD4^+$ T cells compared to healthy controls (Supplementary Fig. S14A). 19M C57BL/6 mice in all these conditions had lower splenic $CD4^+$ T cells compared to 4M group (Supplementary Fig. S14A). Splenic $CD4^+CD44^+$ cells were similar between Mtb infected and RIF-INH treated groups in both 4M and 19M C57BL/6 mice (Supplementary Fig. S14B). Total lung $CD4^+$ T cells were low in 19M C57BL/6 mice compared to 4M group (Supplementary Fig. S14C). These lung $CD4^+$ T cells remained similar upon Mtb infection in both the mice age groups (Supplementary Fig. S14C). 19M C57BL/6 mice receiving RIF-INH treatment showed lower lung $CD4^+$ T cells but it remained similar in 4M C57BL/6 mice (Supplementary Fig. S14C). Lung $CD4^+CD44^+$ cells were higher in Mtb infected 4M C57BL/6 mice which reduced with RIF-INH treatment (Supplementary Fig. S14D). These activated lung $CD4^+$ T cells were overall higher than 4M mice, but remained similar before and after Mtb infection as well post RIF-INH treatment (Supplementary Fig. S14D). Next, we focused on CXCR5, PD1 and ICOS marker specific cell subsets in the spleen and lungs of these study groups (Supplementary Fig. S15A). Splenic $CD4^+CD44^+CXCR5^+$ cells remain similar upon Mtb infection in both 4M and 19M C57BL/6 mice but increased upon RIF-INH treatment (Fig. 5J). 19M C57BL/6 mice

infected with Mtb and receiving treament had higher $CD4^+CD44^+CXCR5^+$ cell frequency than younger counterpart (Fig. 5J). Splenic $CD4^+CD44^+CXCR5^+PD1^+$ and $CD4^+CD44^+CXCR5^+PD1^+ICOS^+$ cell frequencies were higher in all groups (H, I and T) of 19M C57BL/6 mice compared to 4M group (Figs. 5K and L). However, 4M C57BL/6 mice receiving treatment had higher $CD4^+CD44^+CXCR5^+PD1^+ICOS^+$ cell frequency (Fig. 5L). Lung $CD4^+CD44^+CXCR5^+$ cell frequency in 4M C57BL/6 mice upon Mtb infection and RIF-INH treatment remained similar whereas it was significantly lower in Mtb infected 19M mice group (Supplementary Fig. S15B). Lung $CD4^+CD44^+CXCR5^+PD1^+$ and $CD4^+CD44^+CXCR5^+PD1^+ICOS^+$ cell frequencies were similar in Mtb infected and RIF-INH treated 4M and 19M C57BL/6 mice groups (Supplementary Figs. S15C and D).

Proteomic profiling of sorted $CD4^+CD44^+$ T splenic cells revealed changes in Mtb infected 19M C57BL/6 mice: To monitor the differences in the proteome of flow sorted splenic $CD4^+CD44^+$ T cells of 4M and 19M mice groups, if any, two sets of TMT10plex experiments were performed (Supplementary Table S1). Equal protein amount (10 µg) of $CD4^+CD44^+$ T cells harvested from Mtb infected (in triplicates) and healthy controls (in duplicates) were included in set-1 and set-2 consisted of Mtb infected (in duplicates) and RIF-INH treated groups (in triplicates) for comparison (Fig. 6A). In TMT set-1 experiment, out of the 109 identified proteins, 23 showed de-regulation ($p \leq 0.1$, $\log_2$fold change: I/H > |0.58|; 18/5: up-/down- regulated) in the activated $CD4^+$ T cells of 4M C57BL/6 mice (Fig. 6B, Supplementary Fig. S16A and Supplementary Table S2). While, in 19M C57BL/6 mice, a set of 30 deregulated ($p \leq 0.1$, $\log_2$fold change: I/H > |0.58|; 21/9: up-/down- regulated) were identified (Fig. 6C). Functional analysis of these deregulated proteins using Metascape showed perturbations in post-translational protein phosphorylation, ribosome biogenesis, regulation of carbohydrate metabolic processes and mitochondrial metabolism. Mitochondrial proteins 4-hydroxy-2-oxoglutarate aldolase, ATP synthase subunit beta were identified (Supplementary Figs. S17A and B). 4-hydroxy-2-oxoglutarate aldolase was down-regulated post Mtb infection in the splenic $CD4^+CD44^+$ T cells of 19M C57BL/6 mice ($\log_2$fold change: I/H = -1.20) and in 4M mice ($\log_2$fold change: I/H = -0.93) compared to respective healthy controls. ATP synthase beta subunit expression in the splenic $CD4^+CD44^+$ T cells of Mtb infected 4M and 19M C57BL/6 mice were similar.

In the TMT set-2 experiment, out of the 41 unique proteins identified, a set of 20 proteins showed deregulation ($p \leq 0.1$, $\log_2$fold change: T/I > |0.58|; 3/17: up-/down- regulated) in 4M C57BL/6 mice receiving treatment (Fig. 6D, Supplementary Fig. S16B and Supplementary

Table S3). While, $CD4^+CD44^+$ T cells of 19M C57BL/6 mice showed 19 deregulated ($p \leq 0.1$, log_2fold change: T/I > |0.58|; 3/16: up-/down- regulated) proteins (Fig. 6E). Mitochondrial aspartate aminotransferase levels were similar (log_2fold change: T/I = 0.3) in Mtb infected 4M C57BL/6 mice whereas significantly higher (log_2fold change: T/I = 1.53) levels of it was observed in RIF-INH treated 19M mice groups compared to their Mtb infected group (Supplementary Fig. S17C).

Discussion

The elderly human population (>60 years) is vulnerable to different infections like TB due to low vaccine protection and age- related immune dysfunction. The aged TB patients present atypically at the time of diagnosis and during treatment may also show varied outcome. Different in vivo models like non-human primates, mice, guinea pigs, and rabbits have been used to understand TB. However, mice were widely used as model system to understand TB pathophysiology. It is important to mention that mice of 6-8 weeks of age which represents human age equivalent of 18-20 years are commonly used[7]. However, Mtb infection-induced alterations with focus to elderly, i.e. >65 years is very limited, and in this study, we used C57BL/6 mice of >17 months of age to monitor Mtb load in affected organs, immune cell frequency, circulatory cytokines, liver micronutrient profile and compared with 8 weeks of mice.

Ageing-associated accumulation of molecular and physiological changes in tissues like the lungs and the overall immune system are well known and persistent lung injury was shown in aged (21 months) mice after sepsis challenge[25,26]. Ageing affects body fat distribution, which contributes to health deterioration and disease susceptibility[27]. The rate of body weight gain in mice, rats and humans is attenuated by age-related metabolic alterations and by external factors like the onset of diseases[28]. In this study, upon Mtb infection, mice of both the age groups (2M, 17M) showed a decline in body weight but significantly higher body weight loss was observed in aged mice. Cachexia, a hallmark of pulmonary TB, is associated with poor prognosis and indicator of adverse treatment outcome[29,30]. We observed that within 2 w.p.t., aged mice partly recovered their lost body weight whereas younger mice took longer duration.

Low aerosol dose (100-120 cfu) of Mtb H37Rv infection was selected in this study to minimize any early deaths in the aged (>17M) C57BL/6 mice groups. With low aerosol dose of Mtb infection, aged and younger C57BL/6 mice showed similar tissue (lung, spleen, and liver) mycobacterial burden up to 6 w.p.i. corroborating earlier reports[8,9]. At 6 w.p.i., aged mice (18M) showed compromised Mtb control and succumbed to the infection compared to young

mice[31,32,33]. Aged (>20M) mice infected with other intracellular pathogens like *Listeria monocytogenes*, *Salmonella typhimurium*, and *Toxoplasma gondii* also reported higher lethality, which clearly indicates the compromised immune system in aged mice, contributing to high lethality[34]. A hematogenous spread of infection from lungs to the liver was reported in 24M B6D2F$_1$ mice[9], but in our study, we observed similar liver mycobacterial load in both the age groups, and it may be due to age and mice strain. Despite the observed similar lung mycobacterial burden between both the age groups, we hypothesized that aged mice might show compromised Mtb clearance upon drug treatment. Interestingly, at initial phase of treatment (i.e. 2 w.p.t.), aged mice demonstrated a delayed Mtb clearance. Such reports on Mtb infection is very limited but similar result of delayed viral clearance was reported in BALB/c mice (17M) infected with PR8 influenza virus[35]. Ageing and drug-associated changes in hepatic function leads to hepatoxicity, and changes in tissue micronutrient levels[14,15]. Aged mice, irrespective of their infection status, showed higher hepatic Cu/Zn and declined Fe/Cu ratios[36]. Accumulation of Cu and Zn in the phagosomes is reported to increase bactericidal activity and help in host defence, but Cu overload is detrimental to the host[37]. Higher liver Cu levels was observed in aged mice, which might be contributing for ineffective Mtb clearance[37]. Anemia due to Mtb pathogenesis lowers the available Fe pool and is a typical host response in counteracting Mtb replication, which was reflected in young mice[38,39]. However, liver Fe levels of aged mice group remain similar with either Mtb infection or RIF-INH treatment. In Mtb infected aged mice, liver Se level was lower than young controls and they partly restored upon treatment. Specific micronutrient supplementation like Zn and Se may have the potential to improve the treatment outcome and hepatoxicity to lead a better quality of life in aged TB patients.

Aged animals, because of a perturbed CD4$^+$ T cell-mediated immunity leads to a poor response of antigen-specific CD4$^+$ T cells[31,40]. A mathematical model predicted higher lung mycobacterial load in aged mice (18M) at 6 w.p.i. compared to 3M mice, partially due to a delayed CD4$^+$ T cell response[41,42]. This delayed emergence of CD4$^+$ T cells in the aged animals could be because of diminished IL-12 response and a compromised IFN-γ production[9,42]. Furthermore, CD4$^+$ T cells in aged mice showed a poor expression of L-selectin and CD11a, which are important for T cell movement across inflamed endothelial blood vessel surfaces[42]. We further investigated the CD4$^+$ T cell profile of spleen and lungs of young and aged C57BL/6 mice. Upon Mtb infection, we observed that the splenic CD4$^+$ T cell count were similar between young and aged (2M and 17M) mice at both 4 and 6 w.p.i.. These observations corroborate with earlier report on low dose Mtb infected C57BL/10 mice of multiple age

groups (3, 6, 12, 24M)[20]. Aged Mtb infected C57BL/6 mice had higher splenic $CD4^+CXCR5^+PD1^+$ cells and low $CD4^+CD44^+CXCR5^+$ cells at 6 w.p.i. compared to healthy controls. Whereas, higher lung $CD4^+CD44^+KLRG1^+PD1^+$ and $CD4^+CD44^+CXCR5^+$ cells were observed in Mtb infected aged mice compared to the younger groups at 4 and 6 w.p.i. respectively.

Limited reports showed the effect of anti-TB drugs in aged mice and on their T cell repertoire with Mtb clearance kinetics. Compromised Mtb clearance in aged mice as observed in this study (Fig. 7) might be due to the impaired T_{FH} cell functionality which was reported earlier in 20M C57BL/6 mice immunized with NP-OVA[43]. At 4 w.p.t., aged mice showed similar splenic $CD4^+CXCR5^+$ cell frequency, with decreased $CD4^+CXCR5^+PD1^+$ cells, suggesting the inability of the host to elicit proper T_{FH} response. T_{FH} cells link the humoral and cell mediated immunity by driving antibody induction during various infections[44]. Ageing causes T_{FH} cell dysfunction and impaired differentiation which compromises the host response against invading pathogens[45]. Recently, T_{FH}-like cells were reported to localize within protective granuloma-associated lymphoid tissue in the lungs of C57BL/6 mice to mediate Mtb control[46]. Low T_{FH} cell frequency with higher expression of inhibitory receptors like Tim-3 and PD-1 was reported in TB patients[47]. Blockade of Tim-3 and PD-1 with monoclonal antibodies restored T_{FH} cell frequency and function ex-vivo[47]. Significantly reduced Mtb antigen induced T_{FH} cell frequency and IL-21 expression was reported in pulmonary TB patients compared to latent TB controls[48]. In other diseases like systemic lupus erythematosus (SLE), Sjögren's syndrome, sarcoidosis and malaria, higher circulating T_{FH} cell frequency was reported[49,50]. Irrespective of Mtb infection or treatment status, higher PD1 expression was observed in the splenic T cells of aged mice, which directly suppresses T_{FH} development[51].

In the validation experiment using 4M and 19M C57BL/6 mice, we included another crucial marker for defining T_{FH} lineage i.e. ICOS. Splenic $CD4^+CD44^+CXCR5^+PD1^+ICOS^+$ cells remain unchanged upon Mtb infection in both 4M and 19M mice groups. These T_{FH} cells increased in 4M mice group post RIF-INH treatment while remain unchanged in 19M C57BL/6 mice, and may be responsible for compromised Mtb clearance. Serum T_H2 cytokine like IL-6 was found to be significantly higher in 19M mice, which reflects higher inflammation in aged mice. Circulatory IFN-γ levels were significantly higher in Mtb infected 4M and 19M groups. TNF-α and IL-1β showed increasing trends upon Mtb infection in both 4M and 19M mice and declined with RIF-INH treatment. IFN-γ and IL-1β have been associated with TB pathogenesis[52]. A study reported increased liver pro- inflammatory cytokines IFN-γ, TNF-α

and IL-1β with declined anti-inflammatory IL-10 and SERPINs in *Salmonella* infected 18M old male BALB/c mice[53].

Since a delay in Mtb clearance from the lungs of >17M mice at 2 w.p.t. was observed, we monitored the functionality of these activated $CD4^+$ T cells of young and aged animals at protein level. Mitochondrial proteins 4-hydroxy-2-oxoglutarate aldolase (HOGA), ATP synthase subunit beta and aspartate aminotransferase (AAT) were identified in this specific T cell population. HOGA and AAT are key mitochondrial enzymes involved in the catabolism of hydroxyproline (Hyp), which is a product of protein degradation[54]. From a series of steps, Hyp is converted to 4-hydroxy glutamate (4-OH-Glu), which forms 4-hydroxy-2-oxo-glutarate (HOG) catalyzed with the help of AAT[54]. The enzyme HOGA converts HOG into pyruvate and glyoxylate[54]. We observed upregulated AAT and downregulated HOGA levels in the splenic T cells, suggesting a buildup of HOG in Mtb infected aged mice. HOG is known to inhibit glyoxylate reductase, leading to the formation for excessive oxalate, which leads to mitochondrial dysfunction in THP-1 cells[55,56].

Few of the limitation of this study are as follows. Monitoring Mtb specific immune responses using tetramer staining or stimulation with Mtb antigenic peptides on harvested immune cells from both age groups were not attempted this study. The study included male C57BL/6 mice, however it would be interesting to capture the details in aged female mice. Cytokines produced in the lung and by particular immune cell subsets would add meaningful information to understand the changes happening in aged mice upon Mtb infection and RIF-INH treatment. Monitoring antibodies in the circulation was also missed in the study. We focused on $CD4^+CD44^+$ cells for proteomics experiments because of low cell numbers of T_{FH} cells sorted. We identified few proteins from the sorted cells, which could be because of less amount of starting material (proteins i.e. 10 µg per TMT vial). Immune cells can be pooled from more animals for sorting enough cells for subsequent proteomics experiments.

This study reports an altered liver micronutrient profile of aged C57BL/6 mice and a delayed lung Mtb clearance, which could be linked to the low splenic T_{FH} cells and their function. Understanding the molecular mechanism that contributes to the alteration in T_{FH} frequency or its impaired function in aged mice might identify novel targets to improve the immune dysfunction. After careful validation, supplementing aged TB patients with specific micronutrients and adopting adjunct therapeutics that target mitochondria to increase the T cell functionality might be useful for efficient pathogen clearance.

Materials and methods

Experimental groups, Mtb infection and treatment: Procedures adopted in this study were performed following the recommended Guidelines for Care and Use of Laboratory Animals and approved by the Animal Ethics Committee of International Centre for Genetic Engineering and Technology (ICGEB), New Delhi (Ref No. ICGEB/IAEC/07032020/TH-10). C57BL/6 male mice of young (2 and 4 months: M) and aged (17 and 19M) groups were procured from ICGEB bio-experimentation facility. These mice were transferred to Tuberculosis Aerosol Challenge Facility (TACF; BSL-3 facility) for infection experiments. Mice were fed chow diet and water ad libitum throughout the experiments and maintained at 20-22 ºC; 45-60 % humidity with 12 h light/dark cycle. Weight adjusted and randomly grouped mice (n=5 per group) were used in the experiments. After 1 week of acclimatization in TACF, mice were infected with a low dose (100-120 cfu) of animal passaged H37Rv strain in Madison aerosol exposure chamber (University of Wisconsin, USA). Phthiocerol dimycocerosates (PDIM) levels of H37Rv strain used for infection experiments were monitored by thin layer chromatography following an earlier report (Supplementary Fig. S18)[57]. Body weight of mice was recorded at multiple time points (pre-infection, 2, 4 and 6 w.p.i. and post treatment) during the experiments. After 2 w.p.i., a subset of mice was treated with RIF (100 mg/L) and INH (100 mg/L) in drinking water and were replaced with fresh drug solutions at every 48 hours. Mouse (n = 1) belonging to 17M group died before completion of 4 w.p.t. and abscess bearing mouse (n = 1) in 17M group were excluded from the study. Under isoflurane anaesthesia, whole blood (500-700 µL) was collected from the mice via retro-orbital puncture. Mice were euthanized by isoflurane overdose followed by cervical dislocation under the supervision of veterinarian and necropsy was carried out. Serum was isolated from whole blood by centrifuging at 2000 × g at 4 °C for 10 min and used for cytokine profiling. Tissues (lung, spleen, and liver) were harvested for bacterial cfu assay and immune cells were isolated at indicated time points. Spleen weight was measured to assess group-specific differences. A part of the tissue was kept in neutral buffered formalin (500 µL, 10 %) for histopathology analysis. A part of liver sample was rinsed with chilled PBS and after putting it in liquid nitrogen, were stored in -80 ºC for subsequent micronutrient profiling using inductive coupled plasma mass spectrometry (ICP-MS).

Bacterial load monitoring by cfu assay: Briefly, the organs (left lobe of lungs, half of spleen, and two third of liver) were homogenized using T-25 digital Ultra-Turrax disperser (IKA, India) in phosphate buffered saline (1 mL). The homogenates were serially diluted and plated in duplicates on 7H11 agar supplemented with Middlebrook OADC (10%, BD Biosciences,

#211886). These plates were incubated at 37 ºC in a humidified incubator and bacterial colonies were enumerated at 3 weeks post inoculation.

Histopathology: Formalin fixed tissues were paraffin embedded and sectioned using a sliding microtome (Thermo Scientific, USA). Tissue sections (5 µm) were stained with Hematoxylin and Eosin (H&E) and were analysed and images were captured at 100/400 × magnification using a light microscope (Nikon Eclipse TS2). Coded individual slides (without the group information) were shared with the pathologist for scoring to minimise the bias. The scoring was based on severity of inflammation i.e. presence or absence of inflammatory cells, granuloma formation and necrosis.

Liver micronutrient profiling: Liver samples (~50 mg) of C57BL/6 mice (2M and 17M) of healthy, Mtb infected and drug treated groups were weighed and transferred to sample vials (MG5, Anton Paar, USA). H_2O_2 (Supelco, # 1.07298.1000, 30% Suprapur; 100 µL) was added along with HNO_3 (Sigma-Aldrich, USA, # 225711; 70%, 400 µL) to the liver samples and the vials were sealed. The sample containing vials were then subjected to microwave (Anton Paar, USA) digestion using: 150W for 10 min, held for 15 min, 250W for 10 min and held for 15 min. After appropriate dilution with double distilled water (Barnstead™ Smart2Pure water purification system, Thermo Scientific, USA), the digested liver samples were introduced to ICP-MS (iCAP™-TQ ICP-MS, Thermo Scientific, USA) using argon as carrier. Briefly, acid digested samples were aspirated using sample capillary (0.55 mm) through a V-grooved Micromist DC nebulizer and spray chamber of ICP-MS. Samples were passed through a quartz torch, with an injector diameter of 2 mm, which produces plasma. Samples were ionized by plasma and passed through sample cones followed by a skimmer cone. The nebulizer flow was set at 1.045 L/min with a pressure of 3.20 bar, the peristaltic pump was revolving clockwise (40 rpm) and instrument exhaust was maintained at 0.47 mbar. Interface temperature was maintained at 30.53 °C with a cool flow of 14 L/min. Nickel sample and skimmer cones with orifice's diameter of 1 mm and 0.5 mm respectively were used. To avoid any polyatomic ion interference, data acquisition was carried out using KED (Kinetic energy dissociation) mode.

ICP-MS data acquisition was carried out using Qtegra (Intelligent Scientific Data Solution software, Thermo Scientific, USA, version: 2.10.4345.39) to monitor ^{57}Fe, ^{63}Cu, ^{66}Zn and ^{77}Se. Following the manufacturer's instruction, calibration plot for ^{57}Fe, ^{63}Cu, ^{66}Zn and ^{77}Se (range 1-1000 ppb) was prepared using different concentrations of multi-element standard mix (Supelco, #92091). To remove carryover between sample runs if any, HNO_3 (1%) was pumped through the nebulizer with a wash-out time of 30 s. During the sample run, a dwell time of 0.1

s was followed. The average value from the three runs were used to calculate the micronutrient levels and exported for further statistical analysis. Using standard curves of micronutrients, the absolute amount of liver micronutrients was calculated for between group comparison.

Tissue processing for immune cell isolation: Harvested tissues (right lobe of lungs/half spleen) of each mouse belonging to 2M/17M age groups were incubated with collagenase D (1 µg/mL, Sigma, #11088866001) and DNase I (0.5 mg/mL, Sigma, #10104159001) in RPMI media 1640 (Gibco, #31800022) at 37 ºC for 30 min. The cell suspension was passed through a cell strainer (70 µm) and centrifuged at 400 × g at 4 ºC for 5 min. The cell pellet was lysed with RBC cell lysis buffer (Ammonium–chloride–potassium (ACK) buffer, 1×, filter sterilized) at room temperature for 5 min. After washing the immune cells with PBS, staining of cell surface markers was carried out.

Lungs and spleen immune cell profiling: Harvested lungs and spleen immune cells were incubated with recommended dilutions of antibodies conjugated to fluorophores: CD3-BV510 (BioLegend, #100234), CD4-BV785 (BioLegend, #100552), CD8-Alexa fluor 700 (BioLegend, #100730), CD44-BV605 (BioLegend, #103047), CXCR5-PE/Dazzle (BioLegend, #145522), PD1-PE-Cy7 (BioLegend, #109110) and KLRG1-BV421 (BioLegend, #138414) along with APC-Cy7-live dead stain (Invitrogen, # L34994) on ice for 45 min. After washing with buffer (0.2 % FBS in 1× PBS) twice, cells were fixed with fixation buffer (1×, 1 mL, Invitrogen, #00-5123) and kept on ice for 30 min. The cells were washed with buffer (0.2% FBS in 1× PBS) and data (~1 million events/sample) was acquired using BD LSRFortressa X-20 (BD Biosciences, USA). The acquired flow cytometry data were analysed using FCS Express (DeNovo software, version 6).

Fluorescence activated cell sorting (FACS): Another set of harvested lungs and spleen immune cells were stained with recommended dilutions of antibodies conjugated to fluorophores: CD3-FITC (Invitrogen, #11-0032-82) CD4-SB600 (Invitrogen, 63-0042-82), CD8a-BV421 (BioLegend, #100753), CD44-BV510 (BioLegend, #103044), CXCR5-PE (BioLegend, #145504), ICOS-PerCP/Cy5.5 (BioLegend, #313518), PD1-PE Cy7 (BioLegend, #109110) along with APC-Cy7-live dead stain (Invitrogen, #L34994) on ice for 45 min. After washing the cells with buffer (3% FBS in 1× PBS) two times, splenic $CD4^{+}CD44^{+}$ T cells were sorted. Immune cell sorting was done using BD FACS Aria III Fusion (BD Biosciences, USA) present in TACF. The entire splenic cells from sample tubes were sorted. The acquired flow cytometry data were analysed using FlowJo (BD Biosciences, USA, version 10.8.1).

Cytokine measurement and analysis: Serum isolated from whole blood samples of healthy, Mtb infected and drug treated C57BL/6 mice of 4M and 19M age groups were used for cytokine measurement. The cytokines: IL-23 (Biolegend, #740151), IFN-γ (Biolegend, #740153), TNF-α (Biolegend, #740154), IL-1β (Biolegend, #740157), IL-6 (Biolegend, #740159) and IL-17A (Biolegend, #740161) were monitored using capture bead-based assay LEGENDplex (BioLegend). The lyophilized standard (BioLegend, # 740371, lot no. B330381) was reconstituted with assay buffer (250 µL) and then diluted four times and a standard plot was prepared for each cytokine. The serum samples were diluted two-fold with assay buffer and the protocol was followed as per manufacturer's guidelines. The flow cytometer was set up with raw and PE beads using PE as the reporter channel and APC as the bead classification channel. The samples (200 µL) were acquired at a flow rate of 0.5 µL/s, with mixing volume (120 µL), mixing speed (180 µL/s) with a BLR period of 5s. The acquired flow cytometry data were analyzed using Qognit (LEGENDplex Cloud-Based software) to monitor group-specific variation.

Protein isolation from sorted splenic $CD4^+CD44^+$ cells: The sorted splenic $CD4^+CD44^+$ cells in TRIzol reagent (Invitrogen, #15596018) were pipetted up and down 2-3 times to homogenize the cell lysate. Chloroform (SupraSolv, Sigma-Aldrich, #1.02432.1000; 150 µL) was added, mixed by inverting the tube and it was incubated for 2-3 min. The sample was centrifuged at 12,000 × g at 4 °C for 15 min. The mixture separates into a lower phenol-chloroform containing protein and DNA, an interphase, and a colorless upper aqueous phase containing RNA. The aqueous phase was transferred to a new tube by tilting the tube at 45° and pipetting the solution out. For protein isolation, absolute ethanol (Supelco, #1.00983.0511; 200 µL) was added to the phenol-chloroform phase, mixed by inverting the tube and it was incubated for 2-3 min. The DNA was pelleted down by centrifuging at 2000 × g at 4 °C for 5 min. The phenol-ethanol supernatant was transferred to a new 1.5 mL tube and isopropanol (Sigma-Aldrich, #I9516; 1 mL) was added, mixed and incubated for 10 min. The proteins were pelleted down by centrifuging at 12,000 × g at 4 °C for 10 min. The supernatant was discarded and the protein pellet was washed using guanidine hydrochloride (Millipore, #1.04220.0100; 0.3 M in 95% ethanol, 1.5 mL). The solution was vortexed and incubated at RT for 20 min. The tube was centrifuged at 7500 × g at 4 °C for 5 min. After washing the pellet twice, it was then washed with absolute ethanol and incubated for 20 min and the tube was centrifuged at 7500 × g at 4 °C for 5 min. The supernatant was discarded and the protein pellet was air dried before resuspend in triethyl ammonium bicarbonate (TEAB, Thermo Scientific, USA, # 90114; 100

mM, 200 µL). The total isolated protein from splenic $CD4^+CD44^+$ cells was quantified using Bicinchoninic acid (BCA) Protein Assay Kit (Pierce, Thermo Scientific, USA, #23225).

TMT10 plex mass tag labeling: Equal amount of proteins (~10 µg) from the cell lysates (splenic $CD4^+CD44^+$) of a set of representative samples (n=10) from three conditions (healthy, Mtb infected and treated groups) of two mice age groups (4M and 19M) was taken in a 1.5 mL centrifuge tube for labeling experiment (TMT10plex Isobaric Mass Tag Labeling Kit, Thermo Scientific, #90113). The protein samples' volume was adjusted with TEAB buffer (100 mM, 100 µL) supplied by manufacturer and protein reduction was carried out by incubating with tris(2-carboxyethyl) phosphine (TCEP, 200 mM, 5 µL) at 55 °C for 1 h. Protein alkylation was done using iodoacetamide (375 mM, 5 µL) by incubating at RT for 30 min. Pre-chilled acetone (Sigma-Aldrich, #650501; 660 µL) was added and incubated at -20 °C for 24 h before centrifuging at 8,000 × g at 4 °C for 10 min and the supernatants were carefully discarded. The precipitated proteins were then resuspended with TEAB (100 mM, 100 µL) and digested using trypsin (Pierce Trypsin Protease, # 90057; 2 µg, 2 µL per tube) by incubating at 37 °C for 16 h in a heating block. The tryptic peptides were incubated with the TMT tags at 22 °C for 1 h. The TMT labeling reaction was stopped by addition of hydroxylamine (5%, 8 µL) and incubated for 15 min at 22 °C. The TMT-labelled peptides from all samples were pooled and dried using SpeedVac at RT. Labeled tryptic peptides (~40 µg) was taken for strong cation exchange chromatography (SCX). Briefly, labeled peptides were dissolved in ammonium formate (SRL, # 540-69-2; 5 mM, 1 mL) and loaded onto a pre-equilibrated SCX column ICAT™ cartridge kit (Applied Biosystems- AB Sciex, USA, #4326752). The peptides were eluted using different concentrations (30, 50, 80, 120, 250, 300, 400, and 500 mM) of ammonium formate and collected as fractions. Initial three (30, 50 and 80 mM) and last two (400 and 500 mM) fractions were pooled and dried in SpeedVac at 22 °C. These SCX fractions (n = 5) were cleaned up using C18 spin columns (Peptide Cleanup Spin Tubes, Agilent Technologies, USA, #5188-2750) and dried using SpeedVac at 22 °C.

LC-MS/MS data acquisition and analysis: Each tryptic TMT-labelled peptide fractions (~6 µg) were resuspended in formic acid (0.1%, 20 µL) and analysed using an Orbitrap Fusion Lumos Tribrid Mass Spectrometer connected to a nano-LC Easy nLC 1200 (ThermoFisher Scientific, Singapore). The peptides were separated at a flow rate of 300 nL/min on C18 pre-column (Acclaim PepMap™ 100, 75 µm × 2 cm, nanoViper, P/N 164946, ThermoFisher Scientific Incorporation) followed by analytical column (Acclaim PepMap™ RSLC C18, 75 µm × 50 cm, 2 µm, 100 Å, P/N ES803) using a gradient of solvent B (95% acetonitrile in 0.1% formic acid) from 5-10% for 0-5 min followed by 35% for 5-95 min and finally, 95% for 95-

130 min and solvent A (0.1% formic acid). The eluted peptides were injected into the mass spectrometer and the MS1 data were acquired in positive ion mode at 120,000 orbitrap resolution with mass range from 400 to 1600 Da. Precursor ions were allowed to fragment using higher-energy C-trap dissociation (HCD) in ion trap (IT) detector with collision energy of 38% in a data dependent MSn Scan acquisition. Precursor ions with +2 to +6 charge and monoisotopic ions were selected. Parent ions once fragmented were excluded for 60 s with exclusion mass width of ±10 ppm.

All 5 raw files were searched against the *Mus musculus* uniprot proteome database (ID: UP000000589; accessed on 01/07/2023; 55,087 protein count) and contaminant protein database (provided by the manufacturer) in Proteome Discoverer software version 2.3 (Thermo Scientific, USA). A maximum of two trypsin cleavages were allowed with a precursor mass tolerance of 10 ppm and fragment mass tolerance of 0.8 Da. TMT10plex +229.163 Da (Lys) at N-termini of peptides and carbamidomethylation +57.021 Da (Cys) at C termini were selected as static modifications. Oxidation +15.995 Da (Met) and acetylation +42.011 Da at N-terminus were selected as dynamic modifications and proteins were identified based on at least two peptides at False discovery rate (FDR) < 0.05. Proteins qualifying the parameters ($\log_2$ fold change $\geq \pm 0.58$; $\log_{10}$ p-value ≥ 1) between study groups were selected as important deregulated molecules.

Statistical Analysis: The body weight, cfu, micronutrients, immune cell frequency data were analyzed by parametric analysis using Student's t-test in GraphPad Prism version 8.4.2 (GraphPad Software, San Diego, CA). All data are presented as mean ± standard deviation (S.D.). A p-value of ≤0.05 was considered as significant at 95% confidence interval and p-value of <0.1 was considered as significant at 90% confidence interval for proteomics data. Information about the sample size and statistical analysis adopted in each experiment have been provided in the individual figure legend.

Acknowledgements: FP is supported by the fellowship from Department of Biotechnology, Government of India. SC is a Shyama Prasad Mukherjee fellow and is supported by Council of Scientific and Industrial Research, Government of India. The core support from International Centre for Genetic Engineering and Biotechnology (ICGEB), New Delhi to RKN is highly acknowledged. Haripriya Priyadarsini, Adyasha Sarangi, Nidhi Yadav, Ashish Gupta and Mothe Sravya are acknowledged for their help and support during the animal experiments. Help from staff of bio-experimentation facility and Tuberculosis Aerosol Challenge Facility (TACF) at ICGEB, New Delhi is acknowledged. TACF is supported by Department of Biotechnology, Government of India. We thank Dr. Anmol Chandele for her insightful

comments and suggestions for revising the manuscript. Part of these research findings were presented in World Conference on Lung Health 2022, Virtual, 8-11 November 2022 organized by The Union and 2nd biennial meeting on Sex Differences in the Immune Systems conference, Virtual, 30 November- 2 December 2022 organized by Trinity College Dublin & Whitehead Institute. Some figures have been created with Biorender.com.

Author Contributions: FP and RKN conceptualized the project. RKN acquired funding, shared resources, and administrated the project. FP and SC carried out animal experiments, immune cell staining, flow cytometry data acquisition. ShiC calculated histopathological scores. FP and RKN analysed the data and wrote the original draft and revised it with the suggestions received from all the co-authors. The manuscript was reviewed and approved by all co-authors.

Competing interests: The authors declare no conflict of interest.

Supporting Information: The article contains supplemental information.

References

1. Castle, S.C., Uyemura, K., Fulop, T. & Makinodan, T. Host resistance and immune responses in advanced age. *Clin. Geriatr. Med.* **23,** 463–479 (2007).
2. Yew, W.W., Yoshiyama, T., Leung, C.C. & Chan, D.P. Epidemiological, clinical and mechanistic perspectives of tuberculosis in older people. *Respirology* **23,** 567–575 (2018).
3. Centers for Disease Control and Prevention. TB Statistics Report (2021). Accessed on 01/02/2023.
4. Negin, J., Abimbola, S. & Marais, B.J. Tuberculosis among older adults – time to take notice. *Int. J. Infect. Dis.* **32,** 135–137 (2015).
5. Caraux-Paz, P., Diamantis, S., de Wazières, B., & Gallien, S. Tuberculosis in the Elderly. *J Clin. Med.* **10,** 5888 (2021).
6. GBD 2019 Tuberculosis Collaborators. Global, regional, and national sex differences in the global burden of tuberculosis by HIV status, 1990–2019: results from the Global Burden of Disease Study 2019. *Lancet Infect. Dis.* **22,** 222–241 (2022).
7. Flurkey, K., Currer, J.M., Harrison, D.E. & Fox, J.G. The Mouse In Biomedical Research. *American College of Laboratory Animal Medicine series. Elsevier, AP: Amsterdam* 637–672 (2007).
8. Orme, I.M. Aging and immunity to tuberculosis: increased susceptibility of old mice reflects a decreased capacity to generate mediator T lymphocytes. *J. Immunol.* **138,** 4414–4418 (1987).

9. Cooper, A.M., Callahan, J.E., Griffin, J.P., Roberts, A.D. & Orme, I.M. Old mice are able to control low-dose aerogenic infections with *Mycobacterium tuberculosis*. *Infect. Immun.* **63,** 3259–3265 (1995).
10. Haynes, L., Linton, P.J., Eaton, S.M., Tonkonogy, S.L. & Swain, S.L. Interleukin 2, but Not Other Common γ Chain–Binding Cytokines, Can Reverse the Defect in Generation of Cd4 Effector T cells from Naive T cells of Aged Mice. *J. Exp. Med.* **190,** 1013–1024 (1999).
11. Vesosky, B., Flaherty, D.K., Rottinghaus, E.K., Beamer, G.L & Turner, J. Age dependent increase in early resistance of mice to *Mycobacterium tuberculosis* is associated with an increase in CD8 T cells that are capable of antigen independent IFN-γ production. *Exp. Gerontol.* **41,** 1185–1194 (2006).
12. Sathiyamoorthy, R., Kalaivani, M., Aggarwal, P. & Gupta, S.K. Prevalence of pulmonary tuberculosis in India: A systematic review and meta-analysis. *Lung India* **37,** 45–52 (2020).
13. Dibbern, J., Eggers, L. & Schneider, B.E. Sex differences in the C57BL/6 model of *Mycobacterium tuberculosis* infection. *Sci. Rep.* **7,** 1–8 (2017).
14. Lossow, K. et al. Aging affects sex-and organ-specific trace element profiles in mice. *Aging (Albany NY)* **12,** 13762–13790 (2020).
15. Thompson, N.P. et al. Anti-tuberculosis medication and the liver: dangers and recommendations in management. *Eur. Respir. J.* **8,** 1384–1388 (1995).
16. Lucena, M.I., Sanabria, J., García-Cortes, M., Stephens, C. & Andrade, R.J. Drug-induced liver injury in older people. *Lancet Gastroenterol. Hepatol.* **5,** 862–874 (2020).
17. Anderson, E.R. & Shah, Y.M. Iron homeostasis in the liver. *Compr. Physiol.* **3,** 315–330 (2013).
18. Boelaert, J.R., Vandecasteele, S.J., Appelberg, R. & Gordeuk, V.R. The effect of the host's iron status on tuberculosis. *J. Infect. Dis.* **195,** 1745–1753 (2007).
19. Winslow, G.M., Cooper, A., Reiley, W., Chatterjee, M. & Woodland, D.L. Early T-cell responses in tuberculosis immunity. *Immunol. Rev.* **225,** 284–299 (2008).
20. Turner, J. & Orme, I.M. Identification of altered integrin α/β chain expression on T cells from old mice infected with *Mycobacterium tuberculosis*. *Exp. Gerontol.* **37,** 907–916 (2002).
21. Henao-Tamayo, M., Irwin, S.M., Shang, S., Ordway, D. & Orme, I.M. T lymphocyte surface expression of exhaustion markers as biomarkers of the efficacy of chemotherapy for tuberculosis. *Tuberculosis* **91,** 308–313 (2011).

22. Lindenstrøm, T. et al. T Cells Primed by Live Mycobacteria Versus a Tuberculosis Subunit Vaccine Exhibit Distinct Functional Properties. *EBioMedicine* **27,** 27–39 (2018).
23. Vu Van, D. et al. Local T/B cooperation in inflamed tissues is supported by T follicular helper-like cells. *Nat. Commun.* **7,** 10875 (2016).
24. Slight, S.R. et al. CXCR5^{+} T helper cells mediate protective immunity against tuberculosis. *J. Clin. Investig.* **123** 712–726 (2013)
25. Lee, S. et al. Molecular programs of fibrotic change in aging human lung. *Nat. Commun.* **12,** 6309 (2021).
26. Huang, X. et al. Endothelial FoxM1 reactivates aging-impaired endothelial regeneration for vascular repair and resolution of inflammatory lung injury. *Sci. Transl. Med.* **15,** eabm5755 (2023).
27. Kuk, J.L., Saunders, T.J., Davidson, L.E. & Ross, R. Age-related changes in total and regional fat distribution. *Ageing Res. Rev.* **8,** 339–348 (2009).
28. Pappas, L.E. & Nagy, T.R. The translation of age-related body composition findings from rodents to humans. *Eur. J. Clin. Nutr.* **73,** 172–178 (2019).
29. Bernabe-Ortiz, A., Carcamo, C.P., Sanchez, J.F. & Rios, J. Weight Variation over Time and its Association with Tuberculosis Treatment outcome: A Longitudinal Analysis. *PLoS One* **6,** p.e18474 (2011).
30. Chang, S.W. et al. Gut Hormones, Appetite Suppression and Cachexia in Patients with Pulmonary TB. *PloS one* **8,** p.e54564 (2013).
31. Orme, I.M. Mechanisms underlying the increased susceptibility of aged mice to tuberculosis. *Nutr. Rev.* **53,** S35–S40 (1995).
32. Turner, J., Frank, A.A. & Orme, I.M. Old mice express a transient early resistance to pulmonary tuberculosis that is mediated by CD8 T cells. *Infect. Immun.* **70,** 4628–4637 (2002).
33. Lafuse, W.P. et al. Psychological stress creates an immune suppressive environment in the lung that increases susceptibility of aged mice to *Mycobacterium tuberculosis* infection. *Front. Cell. Infect. Microbiol.* **12,** 990402 (2022).
34. Louria, D.B., Sen, P. & Buse, M. Age-dependent differences in outcome of infections, with special reference to experiments in mice. *J. Am. Geriatr. Soc.* **30,** 769–773 (1982).
35. Toapanta, F.R. & Ross, T.M. Impaired immune responses in the lungs of aged mice following influenza infection. *Respir. Res.* **10,** 1–19 (2009).
36. Watts, D.L. HTMA Mineral Ratios: A Brief Discussion of Their Clinical Importance. *Trace Elem. Newsletter* **21,** 1–3 (2010).

37. Rowland, J.L. & Niederweis, M. Resistance mechanisms of *Mycobacterium tuberculosis* against phagosomal copper overload. *Tuberculosis* **92,** 202–210 (2012).
38. Cercamondi, C.I. et al. Iron homeostasis during anemia of inflammation: a prospective study of patients with tuberculosis. *Blood* **138,** 1293–1303 (2021).
39. Lounis, N., Truffot-Pernot, C., Grosset, J., Gordeuk, V.R. & Boelaert J.R. Iron and *Mycobacterium tuberculosis* infection. *J. Clin. Virol.* **20,** 123–126 (2001).
40. Akbar, A.N. & Fletcher, J.M. Memory T cell homeostasis and senescence during aging. *Curr. Opin. Immunol.* **17,** 480–485 (2005).
41. Friedman, A., Turner, J. & Szomolay, B. A model on the influence of age on immunity to infection with *Mycobacterium tuberculosis*. *Exp. Gerontol.* **43,** 275–285 (2008).
42. Orme, I.M., Griffin, J.P., Roberts, A.D. & Ernst, D.N. Evidence for a defective accumulation of protective T cells in old mice infected with *Mycobacterium tuberculosis*. *Cell. Immunol.* **147,** 222–229 (1993).
43. Sage, P.T., Tan, C.L., Freeman, G.J., Haigis, M. & Sharpe, A.H. Defective TFH Cell Function and Increased TFR Cells Contribute to Defective Antibody Production in Aging. *Cell Rep.* **12,** 163–171 (2015).
44. Crotty, S. T Follicular Helper Cell Biology: A Decade of Discovery and Diseases. *Immunity* **50,** 1132–1148 (2019).
45. Lefebvre, J.S., Masters, A.R., Hopkins, J.W. & Haynes, L. Age-related impairment of humoral response to influenza is associated with changes in antigen specific T follicular helper cell responses. *Sci. Rep.* **6,** 25051 (2016).
46. Swanson, R.V. et al. Antigen-specific B cells direct T follicular-like helper cells into lymphoid follicles to mediate *Mycobacterium tuberculosis* control. *Nat. Immunol.* **24,** 855–868 (2023).
47. Bosco, M.J. et al. The exhausted $CD4^+$ $CXCR5^+$ T cells involve the pathogenesis of human tuberculosis disease. *Int. J. Infect. Dis.* **74,** 1–9 (2018).
48. Kumar, N.P. et al. Decreased Frequencies of Circulating CD4+ T Follicular Helper Cells Associated With Diminished Plasma IL-21 in Active Pulmonary Tuberculosis. *PLoS One* **9,** e111098 (2014).
49. Kudryavtsev, I. et al. Imbalance in B cell and T Follicular Helper Cell Subsets in Pulmonary Sarcoidosis. *Sci. Rep.* **10,** 1059 (2020).
50. Simpson, N. et al. Expansion of circulating T cells resembling follicular helper T cells is a fixed phenotype that identifies a subset of severe systemic lupus erythematosus. *Arthritis Rheumatol.* **62,** 234–244 (2010).

51. Shi, J. et al. PD-1 Controls Follicular T Helper Cell Positioning and Function. *Immunity* **49,** 264–274 (2018).
52. Novikov, A. et al. *Mycobacterium tuberculosis* Triggers Host Type I IFN Signaling to Regulate IL-1β Production in Human Macrophages. *J. Immunol.* **187,** 2540-2547 (2011).
53. Fernandes, S.E., Alakesh, A., Rajmani, R.S., Jhunjhunwala, S., & Saini, D.K. Aging associated altered response to intracellular bacterial infections and its implication on the host. *Biochim. Biophys. Acta - Mol. Cell. Res.* **1868,** 119063 (2021).
54. Belostotsky, R. & Frishberg, Y. Catabolism of Hydroxyproline in Vertebrates: Physiology, Evolution, Genetic diseases and New siRNA Approach for Treatment. *Int. J. Mol. Sci.* **23,** 1005 (2022).
55. Riedel, T.J. et al. 4-Hydroxy-2-oxoglutarate aldolase inactivity in primary hyperoxaluria type 3 and glyoxylate reductase inhibition. *Biochim. Biophys. Acta* **1822,** 1544–1552 (2012).
56. Patel, M. et al. Oxalate induces mitochondrial dysfunction and disrupts redox homeostasis in a human monocyte derived cell line. *Redox Biol.* **15,** 207–215 (2018).
57. Domenech, P. & Reed, M.B. Rapid and spontaneous loss of phthiocerol dimycocerosate (PDIM) from *Mycobacterium tuberculosis* grown in vitro: implications for virulence studies. *Microbiology (Reading, England)* **155,** 3532-3543 (2009).

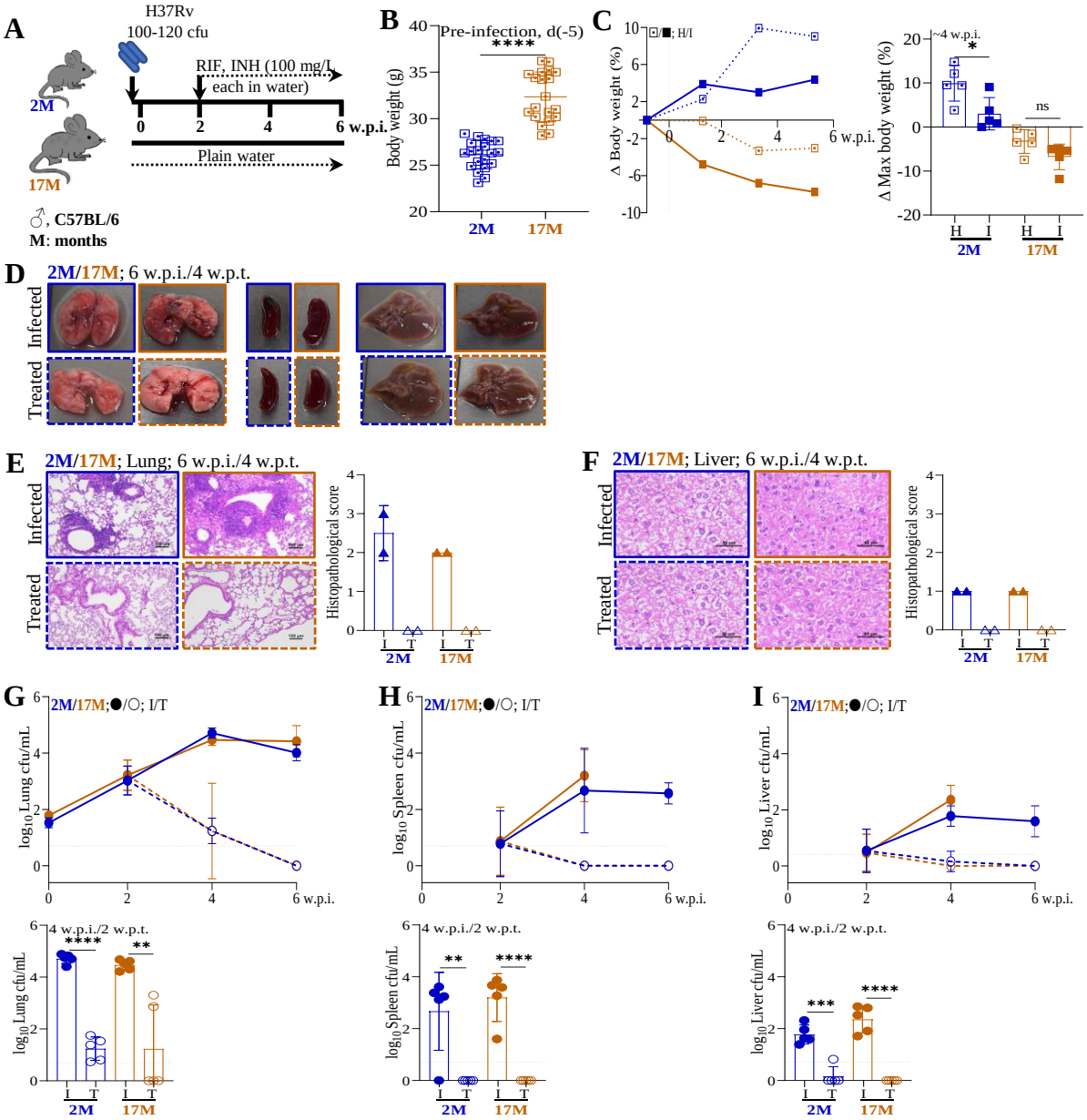

Fig. 1: Aged (17M) C57BL/6 mice receiving two weeks of RIF-INH treatment showed delayed lung Mtb clearance. **A**. Schematic of the experimental details used in this experiment including C57BL/6 mice (male; age groups of 2 and 17 months; M). **B**. Mice (n=20/age group) body weight (in gram) prior to infection (day -5). **C**. Changes in body weight and maximum body weight (%) of mice groups upon Mtb H37Rv infection (healthy: H, ···· ; infected: I, —) are presented as mean of n=5 and individual mice respectively. **D**. Gross pathology of lung, spleen and liver from representative study groups (I, — ; RIF-INH treated: T, – –) at 6 w.p.i./4 w.p.t.. **E**. Histopathological images (hematoxylin and eosin: H&E stained slides) of lung (100× magnification, scale bar=100 µm) and (**F**) liver (400×, 50 µm) of I and T mice groups at 6 w.p.i./4 w.p.t.. The tissue

histopathological scores (w.r.t. healthy, n=2/age group/condition) are presented as histograms. Bacterial burden in the lung (**G**), spleen (**H**) and liver (**I**) of mice belonging to I (at 2, 4 and 6 w.p.i.) and T (at 2 and 4 w.p.t.; treatment started at 2 w.p.i.) groups; dashed horizontal line represents limit of detection (LOD). All bacterial load data points are a mean of n=5/time point/age group/condition, with error bars (standard deviation). n=4 for 17M treated group at 4 w.p.t.. Data points for spleen and liver of infected 17M mice at 6 w.p.i. could not be recorded due to contamination in the plates. The individual data points at 4 w.p.i./2 w.p.t. are presented in histograms. 2M in blue and 17M in brown; p-values: ns = non-significant, * ≤0.05, ** <0.005, *** <0.0005 and **** <0.0001 at 95% confidence interval. *Extended data of this figure are presented in Supplementary Figs. S1-S5.*

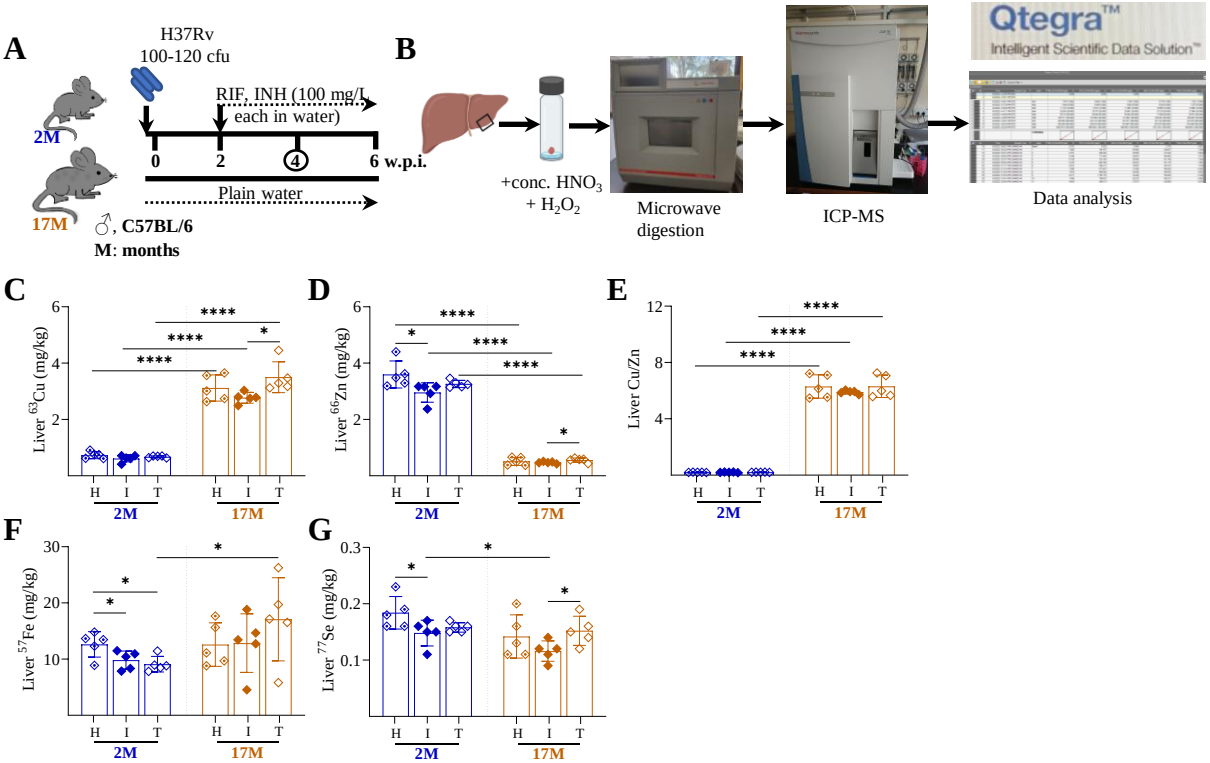

Fig. 2: High liver Cu/Zn in aged C57BL/6 mice was observed which might explain the delayed Mtb clearance at 2 w.p.t.. **A**. Schematic showing Mtb H37Rv infection of C57BL/6 mice of two age groups (2 and 17 in months; M). **B**. Method adopted for liver micronutrient profiling by inductive coupled plasma mass spectrometry (ICP-MS). Abundance of liver micronutrients (in milligram per kilogram): (**C**) copper; ^{63}Cu, (**D**) zinc; ^{66}Zn, (**E**) Cu/Zn ratio, (**F**) iron; ^{57}Fe and (**G**) selenium; ^{77}Se of healthy (H), Mtb infected (I) and RIF-INH treated (T) groups at 4 w.p.i./2 w.p.t. of 2M/17M mice. 2M in blue and 17M in brown; p-values: * ≤0.05 and **** <0.0001 at 95% confidence interval.

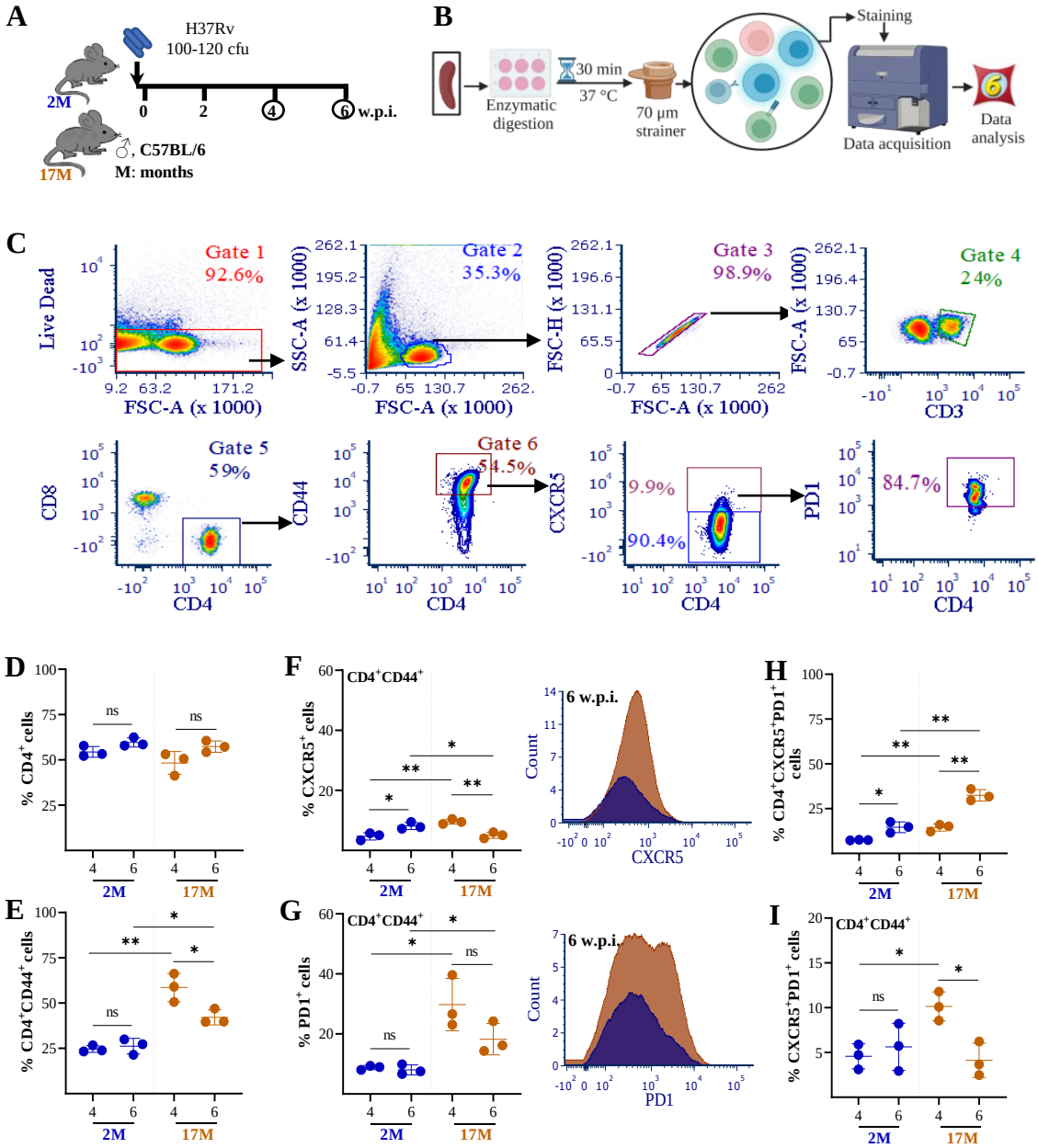

Fig. 3: Splenic CD4⁺CD44⁺CXCR5⁺PD1⁺ cell frequency declined in Mtb infected aged C57BL/6 mice. **A**. Schematic showing Mtb H37Rv infection of C57BL/6 mice of two age groups (2 and 17 in months; M). **B**. Method adopted for lung immune cell isolation, flow cytometry data acquisition and data analysis. **C**. Representative gating strategy followed to monitor the splenic T cell frequencies of Mtb infected mice at 4 and 6 w.p.i.. Frequency of (**D**) $CD4^+$, (**E**) $CD4^+CD44^+$, (**F**) $CD4^+CD44^+CXCR5^+$ with overlay histogram, (**G**) $CD4^+CD44^+PD1^+$ with overlay histogram, (**H**) $CD4^+CXCR5^+PD1^+$ and (**I**) $CD4^+CD44^+CXCR5^+PD1^+$ cells are presented. n = 3/time point/age group; 2M in blue and 17M in brown; p-values: ns = non-significant, * ≤0.05, and ** <0.005 at 95% confidence interval. *Extended data of this figure is presented in Supplementary Fig. S7.*

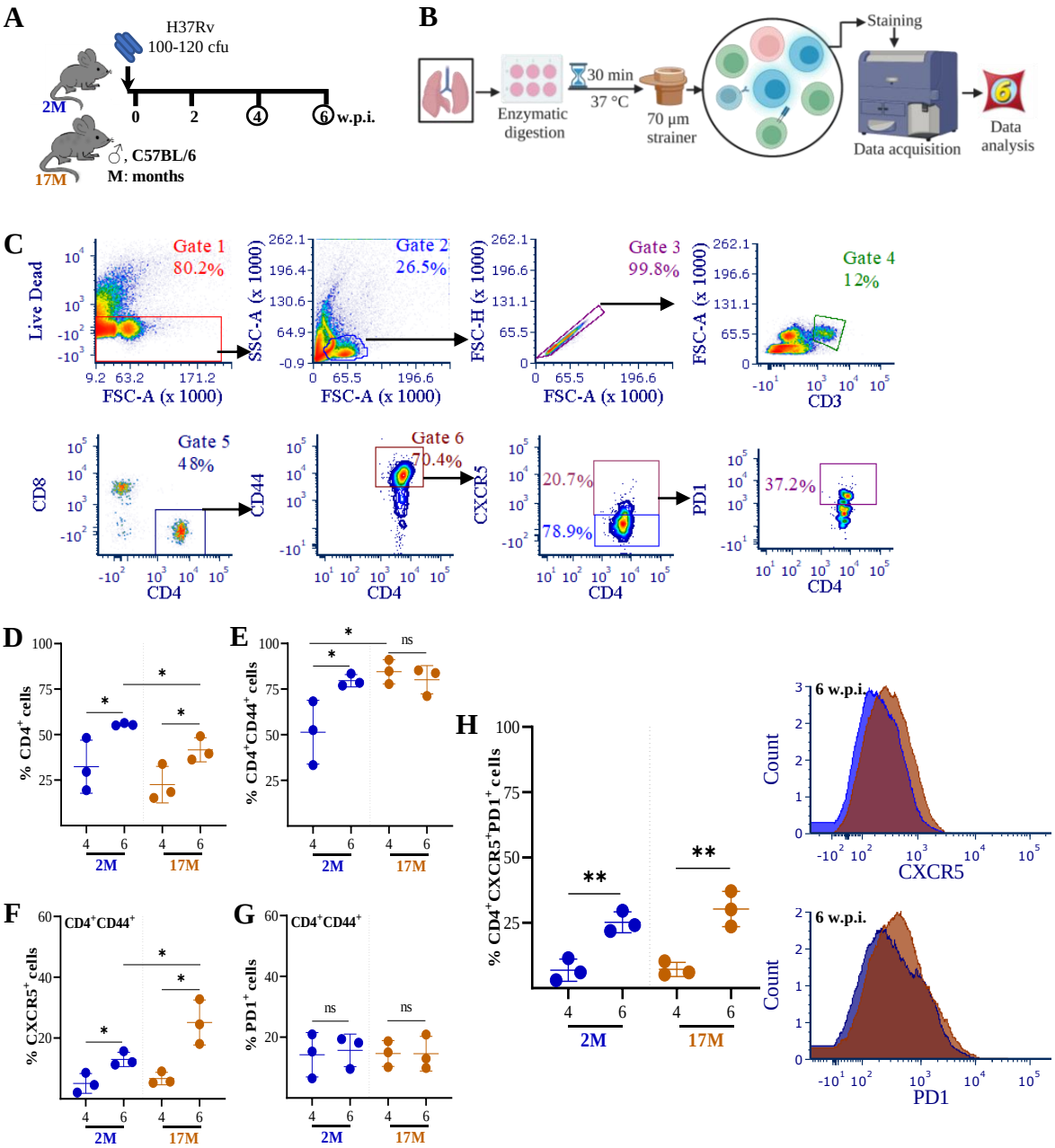

Fig. 4: Lung CD4⁺CXCR5⁺PD1⁺ cell frequency increases in Mtb infected aged and young C57BL/6 mice. **A**. Schematic showing Mtb H37Rv infection of C57BL/6 mice of two age groups (2 and 17 in months; M). **B**. Method adopted for lung immune cell isolation, flow cytometry data acquisition and data analysis. **C**. Representative gating strategy followed to monitor the lung T cell frequencies of Mtb infected mice at 4 and 6 w.p.i.. Frequency of (**D**) $CD4^+$, (**E**) $CD4^+CD44^+$, (**F**) $CD4^+CD44^+CXCR5^+$, (**G**) $CD4^+CD44^+PD1^+$ and (**H**) $CD4^+CXCR5^+PD1^+$ with overlay histograms gated on $CD4^+$ cells are presented. n = 3/time point/age group; M; 2M in blue and 17M in brown; p-values: ns = non-significant, * ≤0.05, and ** <0.005 at 95% confidence interval. *Extended data of this figure is presented in Supplementary Fig. S9.*

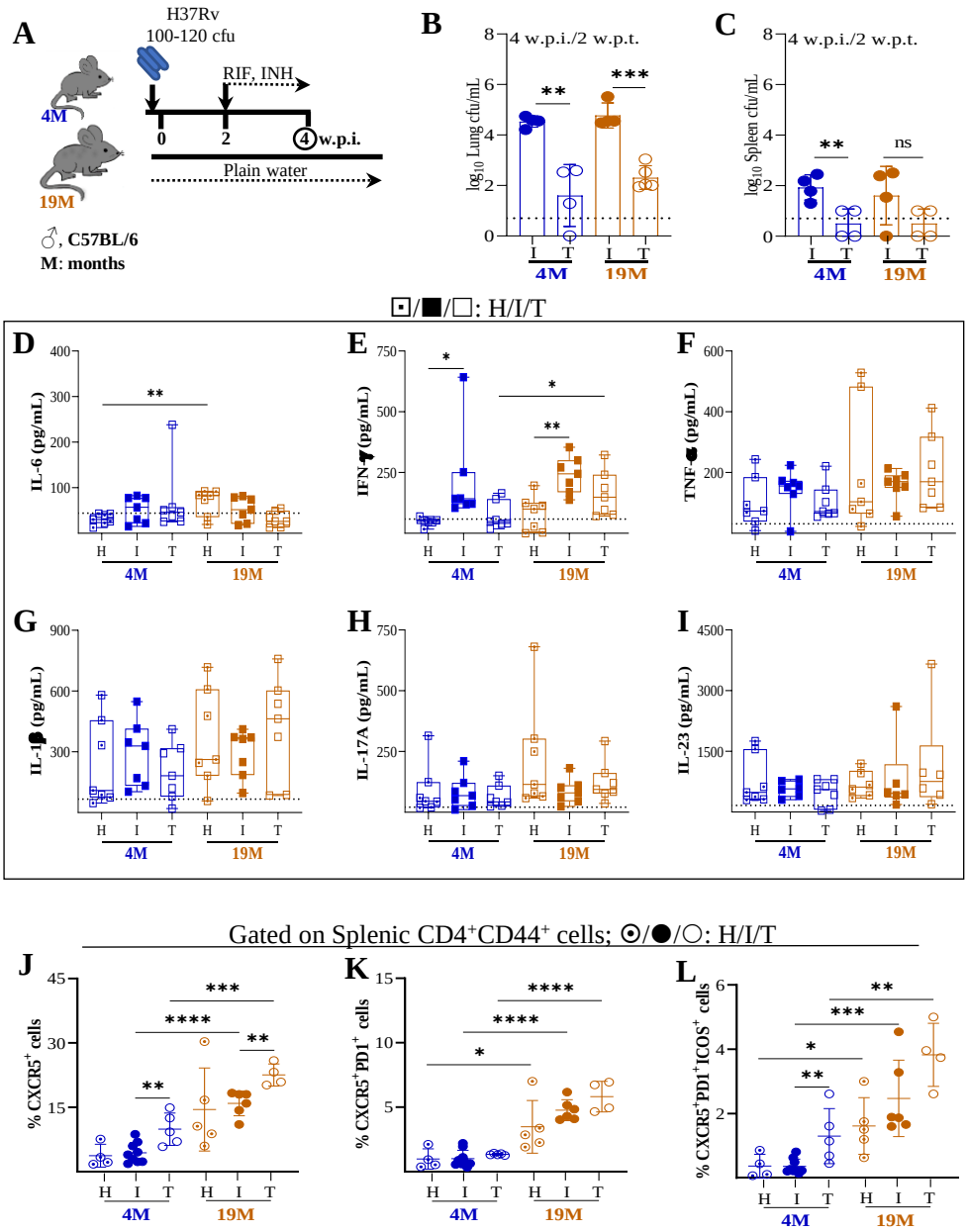

Fig. 5: Higher circulatory IL-6, IFN-γ and splenic CD4⁺CD44⁺CXCR5⁺PD1⁺ cells observed in 19M C57BL/6 mice. **A**. Schematic of the experimental details used for Mtb H37Rv infection of C57BL/6 mice (male, 4 and 19 months; M). Bacterial burden in the (**B**) lung and (**C**) spleen of mice belonging to Mtb infected (I) and RIF-INH treated (T) groups at 4 w.p.i./2 w.p.t. (treatment started at 2 w.p.i.; dashed line represents limit of detection, LOD). All tissue bacterial load data points are presented in the histograms with n = 4/age group/condition, with error bars (standard deviation). Serum cytokines (in picogram per milliliter): (**D**) IL-6, (**E**) IFN-γ, (**F**) TNF-α, (**G**) IL-1β, (**H**) IL-17A and (**I**) IL-23 levels in healthy (H), Mtb infected (I) and RIF-INH treated (T) C57BL/6 mice groups. Frequency of splenic T cells: (**J**) $CD4^+CD44^+CXCR5^+$, (**K**) $CD4^+CD44^+CXCR5^+PD1^+$ and (**L**) $CD4^+CD44^+CXCR5^+PD1^+ICOS^+$ of healthy (H, n=4 for 4M and 5 for 19M), Mtb infected (I, n= 9 for 4M and 6 for 19M) and RIF-INH treated (T, n=5 for 4M and 4 for 19M) C57BL/6 mice at 4 w.p.i./ 2 w.p.t. M; 4M in blue and 19M in brown; p-values: ns = non-significant, * ≤0.05, ** <0.005, *** <0.0005 and **** <0.0001 at 95% confidence interval. *Extended data of this figure are presented in Supplementary Figs. S10-S15.*

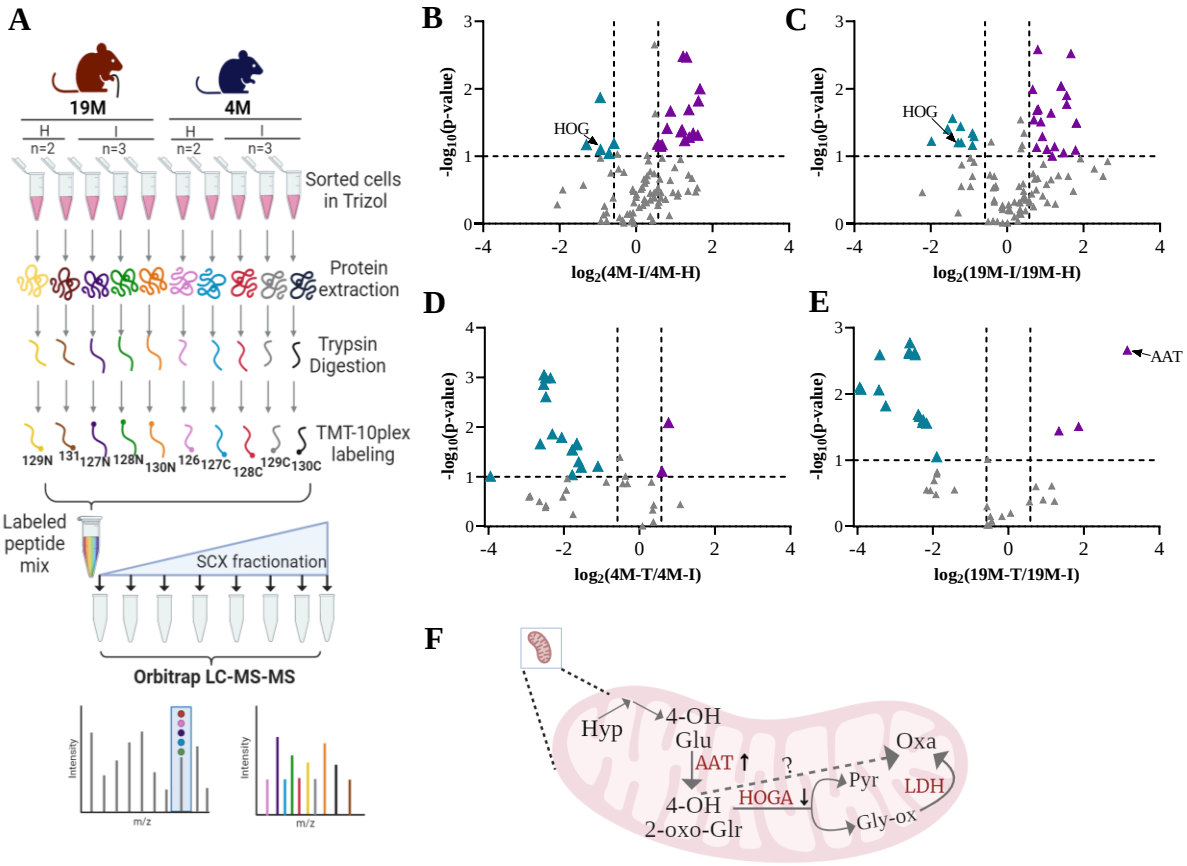

Fig. 6: Deregulated splenic CD4⁺CD44⁺ T cell proteome profile of 4M and 19M C57BL/6 mice upon Mtb infection and RIF-INH treatment. **A**. Schematic representation of method adopted for TMT10plex-T cell proteome analysis (for TMT set-1) by liquid chromatography-mass spectrometry (LC-MS/MS). Volcano plot of CD4⁺CD44⁺ T cell proteome showing significantly deregulated proteins (in $-\log_{10}$ p-value ≥ 1; $\log_2$fold change > |0.58|) in (**B**) Mtb infected 4M versus healthy, (**C**) Mtb infected 19M versus healthy, (**D**) RIF-INH treated 4M versus Mtb infected and (**E**) RIF-INH treated 19M versus Mtb infected mice. **F**. Proteome of splenic CD4⁺CD44⁺ T cells showed alterations in mitochondrial proteins: 4-hydroxy-2-oxoglutarate aldolase (HOGA) and aspartate aminotransferase (AAT) related to hydroxyproline (Hyp) degradation pathway. ▲/▲: up-/down-regulation; H: Healthy, I: Mtb infected, T: RIF-INH treated; M: months. *Extended data of this figure are presented in Supplementary Figs. S16, S17 and Supplementary Tables S1-S3.*

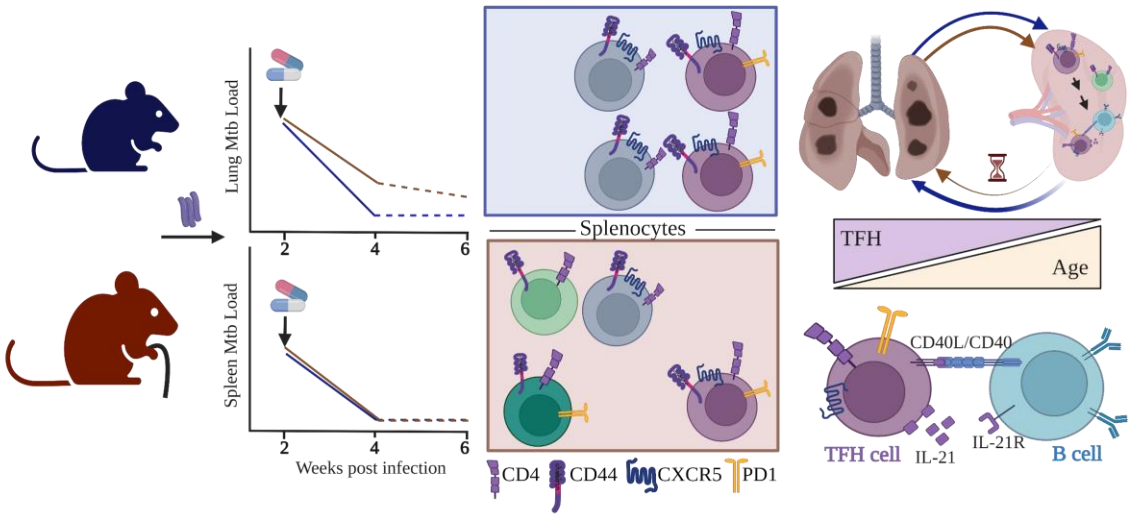

Fig. 7: Aged C57BL/6 mice showed a delayed lung *Mycobacterium tuberculosis* H37Rv (Mtb) clearance in the early time points of rifampicin and isoniazid treatment. Aged mice had low splenic T follicular helper (T_{FH}, $CD4^+CD44^+CXCR5^+PD1^+$) cells, and delayed lung Mtb clearance at 2 weeks post treatment. Also, proteome analysis of splenic $CD4^+CD44^+$ T cells showed alterations in mitochondrial proteins of aged mice. The dysfunctional T_{FH} cells in aged host could be responsible for delayed immune response to Mtb infection.